

Quasiparticle diffusion and the energy resolution of superconducting tunneling junctions as photon detectors. I. Theory

A. G. Kozorezov and J. K. Wigmore

*Department of Physics, Lancaster University, Lancaster, United Kingdom*Roland den Hartog, D. Martin, P. Verhoeve, and A. Peacock
Astrophysics Division, European Space Agency—ESTEC, Noordwijk, Netherlands

(Received 20 July 2001; published 13 September 2002)

One of the factors that degrades the energy resolution of superconducting tunnel junctions (STJ's) as photon detectors at energies above a few keV is the spatial dependence of the response on the photoabsorption site. To assess the role of spatial inhomogeneities we have analyzed quasiparticle diffusion processes in detail and developed a general analytical theory to describe the evolution of the quasiparticle density in an STJ. This theory underlies an analytical model of the STJ response surface, and the corresponding spectral line shape. It accounts for effects of quasiparticle recombination, multiple quasiparticle tunneling, phonon coupling between the electrodes, asymmetry between base and counter electrode, losses at edges and localized traps, and diffusive losses into electrical connections, and is structured such that the effect of these features are added independently, so that the influence of each process can be assessed independently and possible new processes can easily be included.

DOI: 10.1103/PhysRevB.66.094510

PACS number(s): 74.25.Fy, 85.25.Oj, 73.50.Gr, 85.25.Am

I. INTRODUCTION.

Superconducting tunnel junctions (STJ's) are currently being developed as photon-counting spectrometers for a wide range of applications. Their potentially high energy resolution and their capability to handle high count rates make STJ's very promising as photon detectors in an energy range that stretches from near IR to x-ray.¹ The spectroscopic performance of an STJ is conventionally expressed in terms of a full width at half maximum (FWHM) energy resolution ΔE , which comprises several different contributions. Among these contributions are the statistical noise of the number of quasiparticles initially created by the photon absorption (Fano noise²) and of the average number of tunneling events per quasiparticle,^{3,4} considered to be the intrinsic resolution plus the noise from environmental factors (stray IR radiation, read-out electronics, etc.). For Nb/Al based STJ's intrinsic resolution close to the statistical limit has been achieved for photon energies E up to 1 keV.⁵ However, at energies beyond this value the observed ΔE is significantly larger than that calculated from all known contributing factors.

In this paper we consider in detail the suggestion that the excess contribution to the energy resolution arises from variations in the response of the STJ with the position of the photon-absorption site. Experimental support for this hypothesis is found in spatially resolved scans of the response with techniques such as low-temperature scanning electron microscopy (LTSEM) (Ref. 6) and low-temperature scanning synchrotron microscopy (LTSSM) (Ref. 7) and also in the fact that the same detectors have resolutions close to the statistical limit for optical photons.⁸ The energy dependence of the intrinsic resolution would then be explained by the fact that the statistical contributions are proportional to $E^{1/2}$, on account of their Poissonian nature, while any contribution due to spatial variations is proportional to E , because it arises from differences in the magnitude of signals.⁹ Therefore any

spatial contributions tend to dominate at relatively higher energies. Since the future development of STJ's is directed towards low-gap materials, such as Mo and Hf,^{10,11} energy resolution problems due to an inhomogeneous spatial response are expected to become increasingly relevant at lower energies as well.

In order to calculate the effect of inhomogeneous broadening it is necessary to model simultaneously the temporal and spatial evolution of the quasiparticle distribution in both electrodes. From a time-dependent map of quasiparticle density in both electrodes follows the tunneling current as a function of time and photon-absorption position. Integration over time yields the charge output as a function of position, the response surface. The histogram of the response surface gives the corresponding spectral line shape. The time evolution of the quasiparticle and phonon populations is conventionally described by the Rothwarf-Taylor (RT) balance equations.^{9,12,13} However, these equations cannot describe the spatial evolution of the quasiparticle population, for which it is necessary to include the effects of spatial diffusion of quasiparticles. These depend on the specific size, design and structure of the particular STJ under study, especially on the crystallographic quality of the electrodes (e.g., epitaxial or polycrystalline). In addition, quasiparticle dynamics is affected by localized traps, regions of reduced energy gap, presumably introduced at the edges and surfaces during the fabrication process. Finally the size and location of the connecting leads to the electrodes is quite critical, since these are often a major source of quasiparticle loss.

In this paper we present the first, fully analytical theory in which the specific contributions due to all these structural features are taken into account. Earlier work by Refs. 14–16 considered simplified cases describing a single source of loss in STJ's with very specific properties (no phonon coupling between electrodes, no multiple tunneling, or multiple tunneling only between fully symmetric electrodes). Our theory,

on the other hand, allows us to treat the most general case in which all the sources of spatial inhomogeneity can be included separately, taking account of the effects of quasiparticle recombination, multiple quasiparticle tunneling, phonon coupling between the electrodes, asymmetry between base and counter electrode, and the various diffusion processes, several of which were not examined in detail before. The key element of our approach is the way in which the generalized Rothwarf-Taylor equations, containing all the necessary terms relating to inhomogeneous loss, are solved analytically in the quasilinear regime. The major advance is that it allows all different contributions to be entered additively in the calculation of the response surface, and their specific effect on the total energy resolution can be individually assessed. Contributions from possible new processes can be easily included as well.

The outline of the paper is as follows. Section II contains the general description of our approach. The generalized RT equations including all inhomogeneous terms are introduced in Sec. II A. The structure of the solution scheme is given in Sec. II B, resulting in an expression for the response surface. Its relation to the inhomogeneous line broadening is derived in Sec. II C. We discuss the temporal evolution of the quasiparticle population in Sec. II D. The main steps in arriving at the analytical solutions are described in Appendix A. Each of the inhomogeneity generating terms is analyzed separately with the analytic results given in Appendixes B to D. Appendix B relates to inhomogeneity arising from the combined action of the effects of quasiparticle self-recombination, and diffusion in a restricted geometry near the STJ corners and edges. In Appendix C we derive the localized loss terms for the quasiparticles diffusing into leads and bridge connections. The same approach can also be used to describe the effects of local traps. Appendix D deals with imperfectly reflecting edges. Finally Appendix E gives the results on quasiparticle temporal evolution. In the main discussion in Sec. III, we concentrate on the relation between the topology of the response surface and the spectral line shape. We show that the response surface determines all the features of the observed line shapes. We also show that it is possible to relate specific sources of loss to specific features of the response surface and singularities of the line shapes. In the following paper (paper II hereafter,¹⁷) we present two experimental case studies which validate the theory and demonstrate its usefulness.

II. BALANCE EQUATIONS

A. Generalization of the Rothwarf-Taylor equations to include quasiparticle diffusion

The RT balance equations for the temporal evolution of quasiparticle populations in STJ's read

$$\begin{aligned} \frac{dN_i}{dt} &= -N_i\Gamma_{qpl,i} + N_j\Gamma_{t,ji} + 2P_i\Gamma_{phl,i}, \\ \frac{dP_i}{dt} &= -P_i\Gamma_{phl,i} + P_j\Gamma_{pe,ij} + \frac{1}{2}N_i\Gamma_{r,i}, \end{aligned} \quad (1)$$

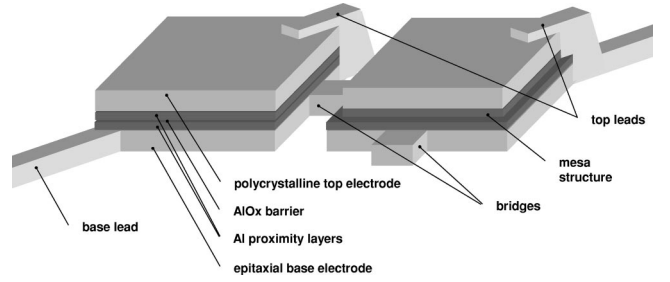


FIG. 1. A schematic representation of STJ's with a definition of their main features. STJ's may be single or, as shown here, connected via bridges into an array. The top electrode of the STJ on the right is smaller than the base electrode. This results in a so-called mesa structure, which leaves a rim in the base electrode from which quasiparticles cannot readily tunnel into the top electrode.

where N_i , P_i are, respectively, the quasiparticle and phonon numbers in electrode i . Here i labels the electrode which absorbs the photon and j labels the counter electrode. In general, $i=1$ indicates the base electrode and $i=2$ the top electrode. We refer to Fig. 1 for a general layout of the STJ and the definition of the relevant parts. The general quasiparticle and phonon loss rates are defined as

$$\begin{aligned} \Gamma_{qpl,i} &= \Gamma_{t,ij} + \Gamma_{r,i} + \Gamma_{l,i}, \\ \Gamma_{phl,i} &= \Gamma_{pe,ij} + \Gamma_{pb,i} + \Gamma_{pl,i}. \end{aligned} \quad (2)$$

Here $\Gamma_{t,ij}$ is the rate at which quasiparticle tunnel from electrode i into electrode j , $\Gamma_{r,i}$ is the quasiparticle recombination rate in electrode i , and $\Gamma_{l,i}$ is the rate at which quasiparticles are lost from electrode i due to trapping. The losses due to quasiparticle diffusion out of the electrode cannot be described in terms of a loss rate and are considered separately. $\Gamma_{pe,ij}$ is the phonon escape rate from electrode i to electrode j , $\Gamma_{pb,i}$ is the rate at which phonons break Cooper pairs to form new quasiparticles, and $\Gamma_{pl,i}$ is the rate at which phonons are lost from electrode i in processes other than escape into electrode j . The quasiparticle recombination rate is given by

$$\Gamma_{r,i} = R_i^*(n_i + 2n_{th}), \quad (3)$$

where under the assumption that $\max\{\Gamma_{pl,i}, \Gamma_{pe,ij}\} \ll \Gamma_{pb,i}$ we can write

$$R_i^* = R_i \frac{\Gamma_{pl,i} + \Gamma_{pe,ij}}{\Gamma_{pb,i}}, \quad (4)$$

where $R_i = (2\Delta/k_B T_c)^3 / [4N(0)\Delta\tau_0]$ is the recombination coefficient,¹⁸ T_c the critical temperature, $N(0)$ the density of states per spin at the Fermi level in the normal state, τ_0 the characteristic time of a superconductor,¹⁹ and n_{th} the density of thermally excited quasiparticles. Splitting the escape routes for recombination phonons with an energy $\hbar\Omega > 2\Delta$ allows us to introduce another convenient quantity, namely the phonon coupling rate $\Gamma_{p,ij}$. By definition, $\Gamma_{p,ij} = \Gamma_{r,i}(1 + \Gamma_{pl,i}/\Gamma_{pe,ij})^{-1}$ is the part of the overall recombination rate in electrode i relating only to the recombination phonons

which escaped through the barrier into the opposite electrode causing pair breaking there. Correspondingly,

$$\Gamma_{p,ij} = R_{ij}^*(n_i + 2n_{th}) \quad (5)$$

with $R_{ij}^* = R_{ij}^*(1 + \Gamma_{pl,i}/\Gamma_{pe,ij})^{-1}$. The phonon loss rate $\Gamma_{pl,i}$ is given in Ref. 20 as

$$\Gamma_{pl,i} = \frac{\eta v_{ph}}{4d_i}, \quad (6)$$

where η is the phonon transmission coefficient through the escape interface, and v_{ph} is the phonon velocity in the medium. These values are weighted averages over the various phonon modes. The phonon transmission through a stack of layers (e.g., Al/AIO_x/Al) can be calculated with the acoustic mismatch model.^{20,21} Because the STJ's are usually operated at temperatures which are typically of the order $0.1T_c$, n_{th} can be neglected in most cases. A direct consequence of Eq. (3) is a quadratic dependence on quasiparticle density, implying that Eq. (1) is nonlinear.

A considerable simplification of Eq. (1) can be obtained by recognizing that phonons do not play a dynamical role in the processes that control the quasiparticle population. First, the velocity of sound in a lattice is typically two orders of magnitude slower than the Fermi velocity,¹⁹ so that diffusion of phonons is negligible compared to quasiparticle diffusion. Second, the phonon pair-breaking time is small compared to other relevant time scales.^{13,19,22} For all materials studied in Ref. 20 the pair-breaking time is about two orders of magnitude smaller than the material constant τ_0 that governs the quasiparticle recombination time. Any phonons that are created with energies larger than 2Δ immediately break Cooper pairs generating pairs of quasiparticles. Hence it is possible to exclude the phonon RT equation and describe phonon transport between the electrodes by effective phonon coupling terms.

In order to describe the spatial variation of the STJ response it is necessary to include the effects of quasiparticle diffusion in the RT equations, and we therefore replace Eq. (1) with the following equations:

$$\begin{aligned} \left. \frac{\partial n_i}{\partial t} - D_i \Delta n_i = -n_i \Gamma_{qpl,i} + n_j \frac{d_j}{d_i} (\Gamma_{t,ji} + \Gamma_{p,ji}) + \frac{\partial n_i}{\partial t} \right|_{\text{diff}} \\ + \frac{N_0}{d_i} \varphi(\mathbf{x} - \mathbf{x}_a) \delta(t), \\ \left. \frac{\partial n_j}{\partial t} - D_j \Delta n_j = -n_j \Gamma_{qpl,j} + n_i \frac{d_i}{d_j} (\Gamma_{t,ij} + \Gamma_{p,ij}) + \frac{\partial n_j}{\partial t} \right|_{\text{diff}}. \end{aligned} \quad (7)$$

We point out that Eq. (7) is written in terms of quasiparticle area densities, thus implying that diffusion takes place only in the plane of the STJ, and that it contains the spatial derivative terms in the balance equations. The second term on the left-hand side describes quasiparticle diffusion inside either electrode, while the third term on the right-hand side represents quasiparticle diffusion out of the electrode via leads, bridges or into localized traps. We also introduced a

pointlike source term describing instantaneous generation of N_0 quasiparticles at $t=0$ with the spatial profile

$$\varphi(\mathbf{x} - \mathbf{x}_a) = 1/(\pi r_{ini}^2) \exp[-(\mathbf{x} - \mathbf{x}_a)^2/r_{ini}^2] \quad (8)$$

inside a small excitation spot of radius r_{ini} around the absorption site with the coordinate \mathbf{x}_a . The magnitude of r_{ini} is estimated in Ref. 23 (from measurements in a Ta absorber) to be of the order of $3 \mu\text{m}$. We have no reason to assume it will be strongly different for Nb. In practice, r_{ini} exceeds the thickness of most electrodes by an order of magnitude. Moreover, the energy gap is uniform in the vertical direction, even when it consists of several layers of different materials, as long as the thickness is smaller than five coherence lengths.²⁴ Again, this is a range in excess of the thickness of most practical electrodes. Therefore we ignore any variation in the vertical reaction and treat the quasiparticle diffusion in the two lateral dimensions. For all linear response problems, however, it is sufficient to take the limit $r_{ini} \rightarrow 0$ resulting in $\lim_{r_{ini} \rightarrow 0} \{1/(\pi r_{ini}^2) \exp[-(\mathbf{x} - \mathbf{x}_a)^2/r_{ini}^2]\} = \delta(\mathbf{x} - \mathbf{x}_a)$. In Eq. (7) we implicitly assume that once diffusion has started, the diffusion constants D_i remain constant. Since the diffusion constant depends on the quasiparticle energy distribution, we therefore assume that the latter does not change significantly after the generation of quasiparticles has completed.

B. Outline of the solution scheme

Here we give a brief outline of the method of solution of Eq. (7); more details are given in appendixes A and B. Since the equations are non-linear, a general exact solution does not exist, and we must therefore look for an accurate approximation. We apply a standard method for the solution of Eq. (7). We expand the solution $n_i(\mathbf{x}, t)$ in a complete, orthogonal system of eigenfunctions $u_{mn}(\mathbf{x})$ of the Helmholtz equation for a square electrode²⁵

$$n_i(\mathbf{x}, \mathbf{x}_a, t) = \sum_{m,n=0}^{\infty} f_{mn}^i(\mathbf{x}_a, t) u_{mn}(\mathbf{x}). \quad (9)$$

The (real) functions $u_{mn}(\mathbf{x})$ are solutions of the dispersion equation

$$\Delta u_{mn} + k_{mn}^2 u_{mn} = 0 \quad (10)$$

with the appropriate boundary conditions at the edges. Through these boundary conditions the various features of the model are introduced: ideal or partially reflective edges or edges with leads, bridges or traps present. Inserting Eq. (9) in Eq. (7), multiplying by $u_{mn}(\mathbf{x})$ and integrating over \mathbf{x} then yields

$$\begin{aligned} \frac{\partial f_{mn}^i}{\partial t} + (D_i k_{mn}^2 + \Gamma_{t,ij} + \Gamma_{l,i}) f_{mn}^i - \frac{d_j}{d_i} \Gamma_{t,ji} f_{mn}^j \\ = \Phi_{mn}^i(\mathbf{x}_a, t) + \frac{N_0}{d_i} \Theta_{mn} \varphi_{mn}(\mathbf{x}_a) \delta(t) + \left. \frac{\partial f_{mn}^i}{\partial t} \right|_{\text{diff}}, \end{aligned} \quad (11)$$

$$\begin{aligned} \frac{\partial f_{mn}^j}{\partial t} + (D_j k_{mn}^2 + \Gamma_{t,ji} + \Gamma_{l,j}) f_{mn}^j - \frac{d_i}{d_j} \Gamma_{t,ij} f_{mn}^i \\ = \Phi_{mn}^j(\mathbf{x}_a, t) + \left. \frac{\partial f_{mn}^j}{\partial t} \right|_{\text{diff}}, \end{aligned} \quad (12)$$

where

$$\begin{aligned} \Theta_{mn} &\equiv \frac{1}{(1 + \delta_{n,0})(1 + \delta_{n,0})}, \\ \varphi_{mn}(\mathbf{x}_a) &\equiv \int_{\text{area}} d\mathbf{x} \varphi(\mathbf{x} - \mathbf{x}_a) u_{mn}(\mathbf{x}). \end{aligned} \quad (13)$$

All nonlinear effects due to quasiparticle self-recombination are combined in the functions Φ_{mn}^i and Φ_{mn}^j :

$$\Phi_{mn}^i(\mathbf{x}, t) = -R_i^* F_{mn}^i(\mathbf{x}, t) + \frac{d_j}{d_i} R_{ji}^* F_{mn}^j(\mathbf{x}, t) \quad (14)$$

with

$$\begin{aligned} F_{mn}^i(\mathbf{x}, t) = \sum_{kl} \sum_{k'l'} f_{kl}^i(\mathbf{x}, t) f_{k'l'}^i(\mathbf{x}, t) \\ \times \int_{\text{area}} d\mathbf{x}' u_{kl}(\mathbf{x}') u_{k'l'}(\mathbf{x}') u_{mn}(\mathbf{x}'). \end{aligned} \quad (15)$$

The integration in Eq. (15) runs over the area of the STJ. For simplicity we have omitted the dependence on \mathbf{x}_a of functions f^i and Φ^i in Eqs. (11), (14), (15). The expression for the function Φ_{mn}^j is given by Eq. (14) where i has to be replaced by j and vice versa. This forms the basis for our solution scheme.

As long as the functions Φ are relatively small (i.e., the system is only slightly nonlinear) we can apply an iterative method to a linearized set of equations. By Fourier transforming the system of differential equations into a system of integral equations it is possible to invert the equations and obtain a formal expression \tilde{f} for the solution. This solution is exact, but contains the self-recombination term Φ , which couples to an infinite number of harmonics of f via nonlinearity. It has the general form $\tilde{f}[\Phi(f^2)]$, which can be calculated to any given accuracy via an iterative scheme. To ensure convergence, f must be small. The first step of the iteration is obtained by taking functions $\Phi=0$, leaving only terms that are linear in the quasiparticle density $\tilde{f}[0]=f_0$. The second order iteration builds on this result, where Φ is taken to its lowest order $\tilde{f}[\Phi(f_0^2)] \rightarrow f_1$. Higher order iterations can be developed similarly.

C. Response surface

Now we consider the charge output $Q_i(E, \mathbf{x}_a)$ of the STJ as a function of photon energy E and photon-absorption position \mathbf{x}_a :

$$\begin{aligned} Q_i(E, \mathbf{x}_a) = e \int_{\text{area}} d\mathbf{x} \int_0^\infty dt [\Gamma_{t,ij} n_i(\mathbf{x}, \mathbf{x}_a, t) \\ + \Gamma_{t,ji} n_j(\mathbf{x}, \mathbf{x}_a, t)]. \end{aligned} \quad (16)$$

This expression can be written as

$$Q_i(E, \mathbf{x}_a) = e N_0 \langle n_i \rangle S_i(E, \mathbf{x}_a) \quad (17)$$

where N_0 is the number of quasiparticles initially generated by the photon and $\langle n_i \rangle$ is the charge multiplication factor (average number of tunneling events for each quasiparticle) due to quasiparticle back tunneling, given by

$$\langle n_i \rangle = \frac{\Gamma_{t,ij}(2\Gamma_{t,ji} + \Gamma_{l,j})}{\Gamma_{t,ij}\Gamma_{l,j} + \Gamma_{t,ji}\Gamma_{l,i} + \Gamma_{l,i}\Gamma_{l,j}}. \quad (18)$$

In Eq. (17) $S_i(E, \mathbf{x}_a)$ is a quantity which we call the normalized response of the device. Plotted as a function of \mathbf{x}_a , it determines the response surface. The density of points on this surface gives the spectral lineshape. We choose the normalization with respect to the ideal case for which all above-mentioned factors causing the response inhomogeneity are absent. For this ideal case $S_i = \hat{1}$, the response surface is a plane and the spectral line a sharp peak.

By applying the iteration scheme to $S_i(E, \mathbf{x}_a)$ we find that $S_i(E, \mathbf{x}_a) = \hat{1} + S_{i,1}(E, \mathbf{x}_a) + S_{i,2}(E, \mathbf{x}_a) + \dots$, where $S_{i,n}(E, \mathbf{x}_a)$ is the n th order iteration for the nonlinear system. For slightly nonlinear systems all the effects resulting in a dependence of the charge output on the coordinates of the absorption site are additive in the lowest order. This means that the effects of quasiparticle recombination may be computed as a series of perturbations on an otherwise ideal system. On the other hand, effects like imperfect reflectivity of the edges or diffusion into leads should, to first order, not depend on nonlinearities. Hence we may compute the effects of sticking at the edges or diffusion into the leads separately for the linear system. In terms of the iteration scheme the response surface thus becomes a linear sum of perturbation surfaces added to the ideal, uniform response surface

$$\begin{aligned} S_i(E, \mathbf{x}_a) = \hat{1} + S_{i,1}(E, \mathbf{x}_a) + S_{i,2}(E, \mathbf{x}_a) + \dots + S_{i,\text{leads}}(\mathbf{x}_a) \\ + S_{i,\text{bridges}}(\mathbf{x}_a) + S_{i,\text{traps}}(\mathbf{x}_a) + S_{i,\text{edges}}(\mathbf{x}_a) + \dots \end{aligned} \quad (19)$$

Here the subscript ‘‘edges’’ indicates the contributions due to a non-ideal reflectivity of the edges. We have dropped the argument E in the response from contributions of edges, leads, bridges and traps because these expressions were obtained within linear theory and are energy independent. In general, $|S_{i,n}| \ll 1$, and $|S_{i,n+1}| \ll |S_{i,n}|$ are necessary conditions for the application of the scheme. The formal expressions for $S_{i,1}(E, \mathbf{x}_a)$ and $S_{i,2}(E, \mathbf{x}_a)$ are derived in Appendix B, those for $S_{i,\text{leads}}(\mathbf{x}_a)$, $S_{i,\text{bridges}}(\mathbf{x}_a)$, and $S_{i,\text{traps}}(\mathbf{x}_a)$ in Appendix C, and that for $S_{i,\text{edges}}(\mathbf{x}_a)$ in Appendix D.

D. Time-dependent solutions

To obtain the dependence of the charge output on time we use Eq. (16) with an finite upper limit in the integral over t . The charge output at a time t is expressed in terms of zero order harmonics as

$$Q_i(E, \mathbf{x}_a, t) = 2e\Gamma_{i,j}d_jL \int_0^t dt' f_{00}^i(\mathbf{x}_a, t') + 2e\Gamma_{i,j}d_jL \int_0^t dt' f_{00}^j(\mathbf{x}_a, t'). \quad (20)$$

In a manner similar to Eq. (19) the solution can be written as

$$Q_i(E, \mathbf{x}_a, t) = Q_{i,0}(E, \mathbf{x}_a, t) + Q_{i,1}(E, \mathbf{x}_a, t) + Q_{i,2}(E, \mathbf{x}_a, t) + \dots + Q_{i,\text{edges}}(E, \mathbf{x}_a, t) + Q_{i,\text{leads}}(E, \mathbf{x}_a, t) + Q_{i,\text{bridges}}(E, \mathbf{x}_a, t) + Q_{i,\text{traps}}(E, \mathbf{x}_a, t), \quad (21)$$

where $Q_{i,0}(E, \mathbf{x}_a, t)$ denotes the solution for an ideal STJ. In Appendix E we present the general framework for the generation of time-dependent solutions.

III. TOPOLOGY OF RESPONSE SURFACES AND CLASSIFICATION OF SPECTRAL LINE SHAPES

In this section we give a general discussion of the solutions to the generalized RT equations in Appendixes A to D. These solutions describe the effects of the various features on the inhomogeneity of the response surface and, correspondingly the shape of the spectral line for monochromatic photons. We consider below the most general case when the base and the top electrodes of the STJ are not identical. Thus, both the case of a high-quality epitaxial base film and a polycrystalline top film as well as the situation in which both films are polycrystalline can be treated within our scheme as limiting cases. However, it is clear that the number of free parameters in these models prohibits any exhaustive exploration of the model. All response surfaces in this section were calculated for realistic sets of STJ parameters, which were derived from fits to experimental data, as will be detailed in paper II.¹⁷ Here, we use the surfaces only for illustrative purposes, as representing a number of distinctive universal topological features. The quantitative scale of the inhomogeneity effects is basically ignored in the treatment here, but will be discussed in detail in paper II.

A. Response surface due to self-recombination

The typical shape of the response surface $S(E, \mathbf{x}_a) = \hat{1} + S_{i,1}(E, \mathbf{x}_a)$ in the first perturbation order is illustrated in Fig. 2(a). The histogram of the points on this surface mimics the experimentally observed line shape, and is given in Fig. 2(b). For photon absorption in the base film the response surface always acquires the shape of a dome with the maximum response being at the geometric center of the STJ. For top film absorption, however, the response surface may acquire the shape of either a dome or an inverted dome shown as in Fig. 3(a), depending on the combination of the major

first iteration for base electrode

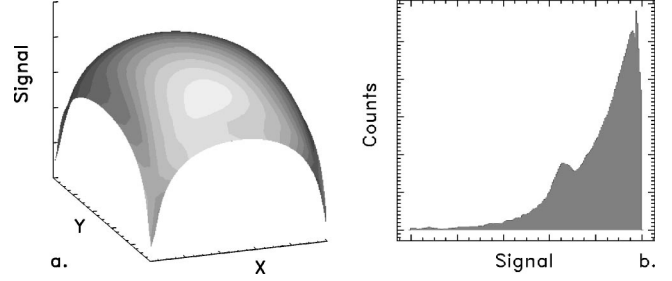


FIG. 2. (a) An example of the contribution to the response surface from the first iteration step. The dome shape is typical for the base electrode. All scales are in arbitrary units, since these depend critically on the input parameters. (b) The corresponding spectral line shape.

STJ parameters (ten in total: two diffusion parameters, four tunnel and loss times, two recombination coefficients, and two phonon coupling parameters). Both dome-shaped and inverted dome-shaped surfaces possess zero-curvature points at the geometrical center of the structure. As a result the corresponding line shapes in Figs. 2(b) and 3(b) show a sharp vertical drop on the right (left) with an extended low (high) charge tail. There are also small secondary bumps in these line shapes (respectively, at 0.65 and 0.35 in the arbitrary units along the horizontal axis). These are due to the topology of the response surfaces close to the values of the response where the connectivity of equal-response contours breaks and instead of one we get four equal-response contours at the corners of the STJ. Equal-response contours are cross sections of the response surfaces in Figs. 2(a), 3(a) in the horizontal plane. While we approach the limiting connected contour from the center of the response surface, the density of points along the one-dimensional sections of the contour close to the centers of the edges rise due to the nearly zero curvature along the edge. At even larger distances from the center, these contributions disappear again, causing a decline of the density.

The physical reason for the dome shape following absorption in the base film is that, because of confinement effects, the quasiparticle diffusion near the edges and corners is slower than diffusion in the bulk of the STJ. As a consequence, the self-recombination of quasiparticles is significantly stronger near the edges, and particularly in the corners of the STJ, and a quasiparticle cloud created following pho-

first iteration for top electrode

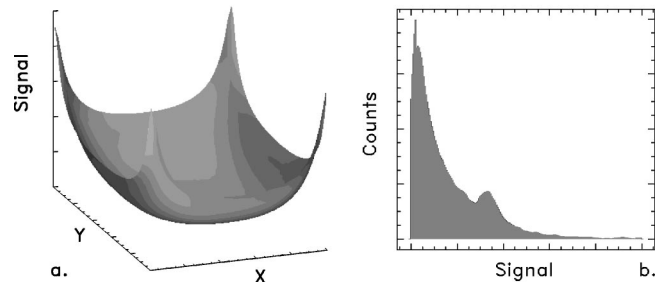


FIG. 3. Another example of the contribution to the response surface from the first iteration step. The inverted dome shape may occur in the top electrode.

ton absorption in the corner suffers larger losses than a cloud created in the center of the STJ.¹³ The inverted dome shape occurs when the quality of base and top films is very different, for example when the top electrode is polycrystalline, while the base is epitaxial. In this case we expect a corresponding difference in the quasiparticle diffusion constants and lifetimes. The inverted dome shape occurs only for the electrode with the slowest diffusion, in this case the top film. Strong self-recombination near the edges and corners transfers a considerable fraction of the generated quasiparticles from the top film to the base film via direct phonon coupling. Because quasiparticles survive longer in the base film, the overall charge output becomes larger for absorptions close to the edges and corners of the top electrode. The response surface also becomes flatter because of the slower diffusion in the top electrode. Finally, the response may become larger than unity and slightly superlinear, in the sense that the non-linearity present in the system brings about a rapid transfer of quasiparticles to the electrode where the contribution to the charge output per quasiparticle is larger. Thus the necessary conditions for the observation of the inverted dome response shape are a significant difference in quality of the electrodes $\langle n_i \rangle \ll \langle n_j \rangle$, and quasiparticle diffusion $D_i \ll D_j$, and a strong phonon coupling.

The inverted dome shape of the response surface due to self-recombination might be turned to our advantage if it could be designed deliberately into an STJ in order to balance the dome-shaped response surfaces which are the contributions from other inhomogeneity factors (see below). Apart from narrowing the line and giving better resolution this might also contribute to a balancing of the STJ nonlinearity over some chosen photon energy range. In particular, if \bar{R}_{ij} can be made zero, the STJ response becomes perfectly linear over the range of energies where second order effects are negligible. Perfect linearity therefore requires that

$$\frac{\langle n_j \rangle}{\langle n_i \rangle} = \frac{R_{ij}^*}{R_i^*} = 1 + \frac{\Gamma_{pl,i}}{\Gamma_{pe,ij}}. \quad (22)$$

The phonon escape rates depend on the quality of the interfaces between the various layers in the STJ and are difficult to modify, but the average number of times that a quasiparticle tunnels can be influenced, for instance, by tuning the thickness of the Al proximity layers.²⁶

Finally, changing the parameters of the STJ can produce a very interesting transformation of the response surface for top absorption from dome-shaped to inverted dome-shaped with an intermediate form shown in Fig. 4(a). Here, in addition to the central spot with zero curvature, there appear as many as eight other features [four saddle points and four minima in Fig. 4(a)] of zero curvature, giving rise to other sharp features of the line shape. The sharp drops on both sides of the line are due to the minima and maximum and the discontinuity of the derivative in the central part of the line. It is interesting that the transformation from dome to inverted-dome topology occurs over a very small range of the loss time in the top electrode—the parameter to which the shape of the response surface turns out to be extremely sensitive in this transition range.

first iteration for top electrode

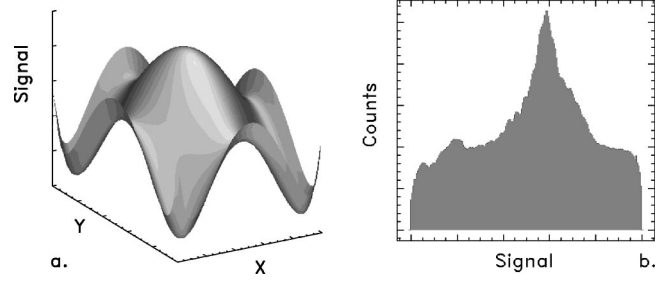


FIG. 4. Another example of the contribution to the response surface from the first iteration step. The inverted tulip shape may occur in the top electrode under special circumstances.

The second-order contribution to response due to self-recombination at any point of the STJ is of different sign (see Appendix B), demonstrating the sign alternating behavior of the iteration series. As a result the second order contribution has an inverted shape in comparison with that of first order. An essential condition for the application of this scheme is that the magnitude of the second-order correction is significantly smaller than the first-order correction. Thus, in all applicable cases, the exact shape of the second-order correction is of no practical interest.

B. Effect of leads, bridges, and traps on the response surface

In general, leads and bridges have the largest impact on the response surface, see, e.g., Ref. 6. In the expressions for the response surface derived in Appendix C, each lead and bridge (or trap) is described by a single quality parameter which incorporates both geometric effects and quasiparticle loss efficiency inside the lead or bridge. The experimental data on leads and bridges plugged with higher-gap material do not always show an 100% efficient Andreev reflection.²⁷ But even in the case of effective Andreev reflection, the lead mouth may become an area of strong quasiparticle recombination, causing the formation of a local spot with enhanced quasiparticle losses. The lead thus acquires traplike qualities. We emphasize that the same expressions as Eq. (C7) can be used to describe the effect of local traps attached to the edge at a random location with the coordinate \mathbf{x}_{trap} . In this model of a local trap, the parameter similar to g_l will measure the “strength” of the trap. In fact, it is clear from the analysis in Appendix C that “lossy” leads and bridges and local traps are objects of the same one-parameter family, and are all characterized by a single strength g .

Figure 5(a) illustrates the effect of an (unplugged) lead in the corner of the STJ and two bridges in the centers of the two sides of the base electrode. Due to the symmetry of lead and bridge connections in the base film the response shape is quite symmetric although the lead connection at the top film causes a little distortion. The response surface possesses almost flat regions in all corners except in the one where the lead is present. Again due to symmetry considerations the elevation of the points in the corner opposite to the lead is smaller than that of the other two corners. The result is the double-peaked line shape shown in Fig. 5(b). The extended

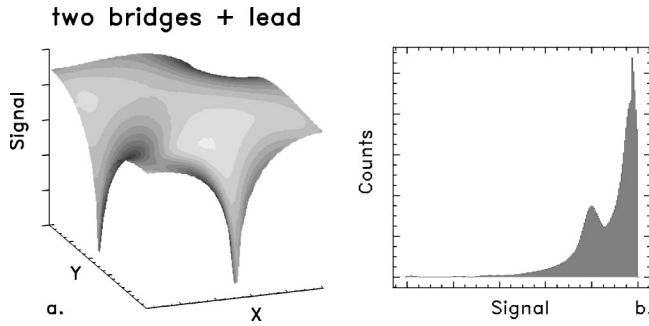


FIG. 5. An example of the contribution to the response surface of the base electrode from two bridges and one lead in the corner. Note the double-peaked lineshape which occurs even when the detected photons are perfectly monochromatic.

low charge tail is due to the lead connection, while sharp drop on the right is due to the last symmetry spot, corresponding to the large flat central part of the response surface, which is most distant from all degrading factors and hence spawns the largest response. The double-peaked line shape is a consequence of the topology of the response surface and occurs even for a perfectly monochromatic input of photons. Finally, Fig. 6(a) shows the effect of a local trap, comparable in strength to the bridges, and located at the edge of the STJ. The response surface here was calculated for the same set of STJ parameters as used for Fig. 5(a). Removal of the flat part of the response surface at the corner where the local trap is located causes a redistribution in the weight of the lines in the double peak, although the double-peak structure itself survives. The overall charge output becomes noticeably smaller with the simultaneous line broadening, and the energy resolution degrades considerably. This illustrates an important general principle in the relation between the topology of the response surface and the width of the spectral line: the stronger the symmetry of the response surface is broken, the broader the spectral line becomes.

C. Effect of imperfect edges on the response surface

The general expression for the response surface due to quasiparticle losses at the edges has been derived in Appendix D. The effect of imperfectly reflecting edges was previously studied for the limiting cases of a single electrode in Ref. 14 and identical electrodes in Ref. 16. In both cases the

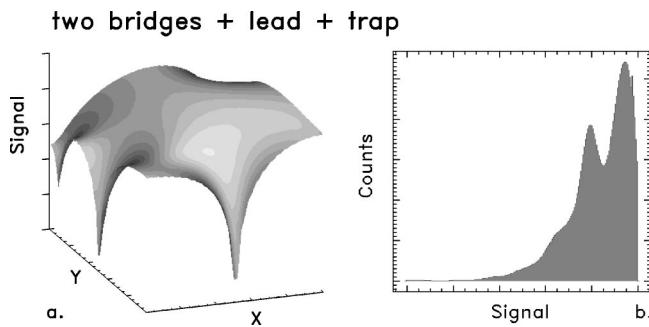


FIG. 6. Same configuration as in Fig. 5, but now with a strong trap added at the location $(-0.5L, +0.4L)$.

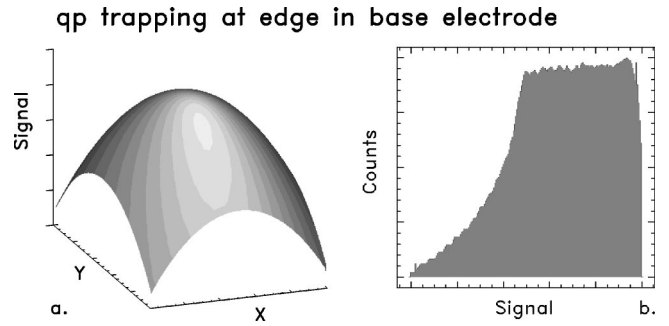


FIG. 7. An example of the contribution to the response surface from nonideal edges. The dome shape is the usual topology.

authors demonstrated the dome-shaped surfaces for the STJ response similar to the surface shown in Fig. 7(a). Our formalism given in Appendix D is more general than the results of Refs. 14,16 and allows us to model STJ's with arbitrary base and top films. Despite the superficial similarities between Figs. 2(a) and 7(a), the actual curvature and shape of the dome is different for this situation compared to that of the self-recombination induced effect. This is best seen in the shape of the spectral lines, which are markedly different.

The topology of the response surfaces and corresponding line shapes for the STJ with different edge quality parameters in the base and in the top films can be completely different from the simple dome shape. Figure 8 illustrates the fact that for an STJ with different edge reflectivities for base and top electrodes, the response surface acquires a tulip shape with a totally different set of symmetry points. The necessary condition for the tulip shape of the response is a large difference in the edge-quality parameters $\beta_i \ll \beta_j$ for base and top electrodes. Apart from the central spot of zero curvature which accounts for the sharp drop on the left of the line there appears a sharp feature, a discontinuity of the derivative in the center of the line due to four saddle points at a small distance from each side center. The sharp drop on the right is due to the four zero curvature spots near the corners of the electrode.

The model of imperfect edge reflectivity used in Refs. 14,16 and in Appendix D assumes homogeneous quasiparticle losses at the perimeter of the electrode. Now, the question

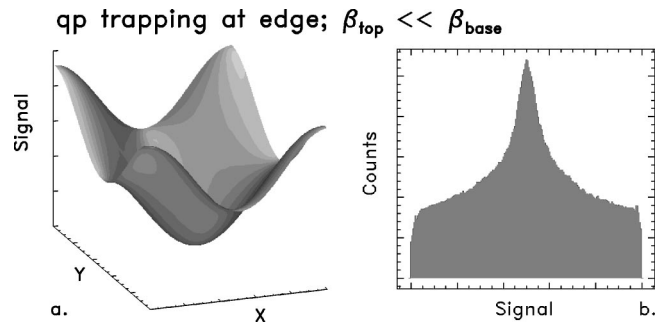


FIG. 8. Another example of the contribution to the response surface from non-ideal edges. The tulip shape may arise when the edge losses in the counter electrode are much larger than in the electrode of absorption.

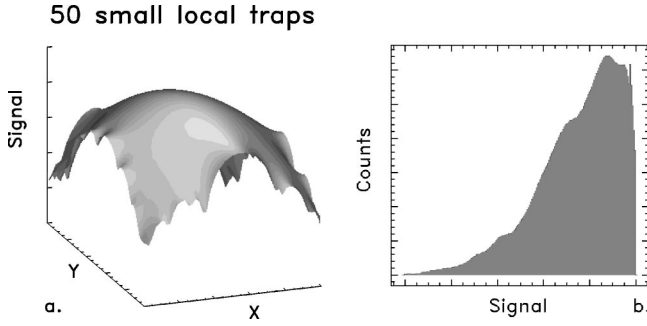


FIG. 9. An approximation of the dome shaped response surface, typical of nonideal edges, arising from a large number (50) of randomly positioned local traps, with randomly distributed strengths.

arises what physical phenomena could underlie the concept of homogeneous losses at the perimeter.

One special case where the concept of homogeneous losses at the edge can be fully justified is that of the base electrode in a mesa structure as shown in Fig. 1. Here the base electrode is slightly larger in size than the top electrode, leaving a narrow rim around the perimeter from which quasiparticles cannot directly tunnel into the top electrode. If there exists a bulk loss mechanism for quasiparticles, then a quasiparticle which approaches the edge in the base film spends some time in the rim without access to barrier. As quasiparticles have a finite probability to get lost during their random walk through the rim, this situation is clearly equivalent to a base electrode without a rim, but with an imperfectly reflecting edge. Of course, this model implies perfectly reflecting edges for the top electrode. We will encounter this situation in practice in paper II. It is interesting to note that for the corresponding choice of STJ parameters in this model, the response surface is dome-shaped for photon absorption in the base electrode and tulip shaped for absorption in the top electrode.

Usually, it is assumed that imperfectly reflecting edges are a limiting case of a situation in which the perimeter contains many small local traps. Oxidation of the Nb at the edge of the electrode may result in small sites that are either superconducting with a small gap (NbO) or normally conducting. Provided that these sites cause the immobilization (or loss) of quasiparticles, and are present in a sufficient large number, they could give rise to an effect that resembles an imperfect edge. This is illustrated in Fig. 9, where 50 small, randomly located local traps, with randomly distributed strengths, do indeed seem to give rise to a dome-shaped response surface as seen in Fig. 7. We finally note that experimental evidence for local traps at the perimeter of a top electrode was found in LTSEM scans,⁶ although the traps did not seem to occur in the numbers assumed for Fig. 9.

IV. CONCLUSIONS

We have developed a theory for the degradation of energy resolution in STJ's. This theory connects the diffusive properties of quasiparticles with the spatial inhomogeneity in the response of the STJ to the absorption of a photon. The topology of the STJ response surface contains the complete infor-

mation of the effect of various factors that cause the inhomogeneity of the STJ response. In the absence of strong nonlinearity all factors contributing to the inhomogeneous line broadening are additive. This theory provides therefore a basis for the reconstruction of observed line shapes and the identification of the origin of different spectral features. It includes the effects of quasiparticle recombination, multiple quasiparticle tunneling, phonon coupling between the electrodes, asymmetry between base and counter electrode, losses at edges and in localized traps and diffusive losses into electrical connections. Because it shows quantitatively the extent of the resolution degradation due to the various factors, it can be used as a diagnostic tool to assess the quality of STJ's—its edges, corners, lead and bridge connections, edge trapping efficiency, local traps, etc., and to explore directions of optimization of the STJ performance. A detailed experimental study illustrating the quantitative description based on the results in this paper and supporting the conclusions in this section is presented in the follow-up paper.

APPENDIX A: SOLUTION OF THE BALANCE EQUATIONS

To solve the set of coupled balance equations (7) we expand the unknown solution $n_i(\mathbf{x}, t)$ in a complete, orthogonal system of eigenfunctions $\{u_{mn}(\mathbf{x})\}$ (9). The functions $u_{mn}(\mathbf{x})$ are solutions of the Helmholtz equation for a square STJ (10) with the proper boundary conditions at the edges (ideal, sticky or with leads, etc). The task is now to find the functions $f_{mn}^{i,j}(\mathbf{x}_a, t)$. We do this by transforming the system of differential equations (11) into a system of integral equations for the Fourier transforms of the $f_{mn}^{i,j}(\mathbf{x}_a, t)$, which we denote $\tilde{f}_{mn}^{i,j}(\mathbf{x}_a, \omega)$. Solving the Fourier transformed system of equations (11) yields

$$f_{mn}^i(\mathbf{x}_a, \omega) = - \frac{A_{mn}^i(\mathbf{x}_a, \omega)}{(\omega + i\epsilon_{mn}^+)(\omega + i\epsilon_{mn}^-)}, \quad (\text{A1})$$

where we have used the following definitions:

$$A_{mn}^i(\mathbf{x}_a) = \Theta_{mn} \left\{ (-i\omega + B_{mn}^j) \left[\Phi_{mn}^i + \frac{N_0}{2\pi d_i} \tilde{u}_{mn}(\mathbf{x}_a) \right] + \frac{d_j}{d_i} \Gamma_{t,ji} \Phi_{mn}^j \right\},$$

$$A_{mn}^j(\mathbf{x}_a) = \Theta_{mn} \left\{ (-i\omega + B_{mn}^i) \Phi_{mn}^j + \frac{d_i}{d_j} \Gamma_{t,ij} \left[\Phi_{mn}^j + \frac{N_0}{2\pi d_i} \tilde{u}_{mn}(\mathbf{x}_a) \right] \right\}$$

$$B_{mn}^i = D_i k_{mn}^2 + \Gamma_{t,ij} + \Gamma_{l,i}$$

$$\epsilon_{mn}^\pm = \frac{1}{2} [B_{mn}^i + B_{mn}^j \pm \sqrt{(B_{mn}^i - B_{mn}^j)^2 + 4\Gamma_{t,ij}\Gamma_{t,ji}}], \quad (\text{A2})$$

where by definition

$$\tilde{u}_{mn}(\mathbf{x}_a) = u_{mn}(\mathbf{x}_a) \exp\left[-\frac{(m^2+n^2)\pi^2 r_{\text{ini}}^2}{4L^2}\right] \approx \varphi_{mn}(\mathbf{x}_a). \quad (\text{A3})$$

For $r_{\text{ini}} \rightarrow 0$ we have $\tilde{u}_{mn}(\mathbf{x}_a) \rightarrow u_{mn}(\mathbf{x}_a)$. We will only use functions $\tilde{u}_{mn}(\mathbf{x}_a)$ different from $u_{mn}(\mathbf{x}_a)$ to treat the self-recombination effects (see below). In all other cases the limit $r_{\text{ini}} \rightarrow 0$ gives an adequate description. Although Eq. (A1) is exact, it is nonlinear through the self-recombination term, which not only couples an infinite number of harmonics via the nonlinear interaction, but also contains an integral over a part of these terms. However, the functions $\Phi_{mn}^{i,j}$ are quadratic in $f_{mn}^{i,j}$, so provided the nonlinearity is small, the solutions of Eq. (A1) can be found via an iterative scheme. The first step of the iteration is obtained by taking functions $\Phi_{mn}^{i,j} = 0$, leaving only terms linear in the quasiparticle density. This leads to

$$\begin{aligned} \tilde{f}_{mn}^i(\mathbf{x}_a, \omega) &= -\frac{N_0}{2\pi d_i} \tilde{u}_{mn}(\mathbf{x}_a) \Theta_{mn} \frac{(-i\omega + B_{mn}^j)}{(\omega + i\varepsilon_{mn}^+)(\omega + i\varepsilon_{mn}^-)}, \\ \tilde{f}_{mn}^j(\mathbf{x}_a, \omega) &= -\frac{N_0}{2\pi d_j} \tilde{u}_{mn}(\mathbf{x}_a) \Theta_{mn} \frac{\Gamma_{t,ij}}{(\omega + i\varepsilon_{mn}^+)(\omega + i\varepsilon_{mn}^-)}. \end{aligned} \quad (\text{A4})$$

The second order iteration is then given by Eq. (A1), where the $\Phi_{mn}^{i,j}$ are taken to their lowest order, which is obtained by substituting result (A4) into Fourier transforms of Eqs. (14) and (15). Higher order iteration steps are built similarly. The convergence for the summations over m, n is ensured by the fact that $\tilde{f}_{mn} \propto (m^2+n^2)^{-2} \exp[-(m^2+n^2)\pi^2 r_{\text{ini}}^2/4L^2]$.

We consider the charge output $Q(E, \mathbf{x}_a)$ of the STJ as a function of photon energy E and \mathbf{x}_a , assuming the STJ to have an ideal edges. In that case the $u_{mn}(\mathbf{x})$ are simple oscillatory functions

$$u_{mn}(\mathbf{x}) = \frac{2}{L} \cos\left[m\pi\left(\frac{1}{2} + \frac{x}{L}\right)\right] \cos\left[n\pi\left(\frac{1}{2} + \frac{y}{L}\right)\right], \quad (\text{A5})$$

where $k_{mn}^2 = (\pi/L)^2(m^2+n^2)$ and L is the size of the STJ. Using Eqs. (9), (16), and (A5) we obtain after integration over STJ area and time

$$\begin{aligned} Q(E, \mathbf{x}_a) &= 4\pi e L [\Gamma_{t,ij} d_i \tilde{f}_{00}^i(\mathbf{x}_a, \omega = 0) \\ &\quad + \Gamma_{t,ij} d_j \tilde{f}_{00}^j(\mathbf{x}_a, \omega = 0)]. \end{aligned} \quad (\text{A6})$$

This expression can be written in the form (17) with

$$\begin{aligned} S_i(\mathbf{x}_a, E) &= 1 - \frac{2\pi}{N_0} \sum_{m,n=0}^{\infty} \Theta_{mn}^{-1} \\ &\quad \times \int_{-\infty}^{\infty} \frac{d_i \tilde{R}_{ij} |A_{mn}^i(\mathbf{x}_a, \omega)|^2 + d_j \tilde{R}_{ji} |A_{mn}^j(\mathbf{x}_a, \omega)|^2}{[\omega^2 + (\varepsilon_{mn}^+)^2][\omega^2 + (\varepsilon_{mn}^-)^2]} d\omega. \end{aligned} \quad (\text{A7})$$

Here we introduced the following notations for the effective recombination coefficients: $\tilde{R}_{ij} = R_i^* - R_{ij}^* \langle n_j \rangle / \langle n_i \rangle$ and $\tilde{R}_{ji} = R_j^* \langle n_j \rangle / \langle n_i \rangle - R_{ji}^*$. The effective recombination coefficients take into account the phonon coupling between the electrodes. This makes it explicit that even in the case of strong self-recombination it is possible to have nearly linear behavior of the charge response, at least for photon absorption in one of the electrodes, when the phonon coupling between the electrodes is properly matched to the quasiparticle tunnel and loss times.

APPENDIX B: NONLINEAR RESPONSE, FIRST AND SECOND ITERATIONS

The first iteration is obtained by the substitution of the linearized solutions $\tilde{f}_{mn}^{i,j}$ (A4) into the expressions for $A_{mn}^{i,j}$ in Eq. (A7):

$$\begin{aligned} S_{i,1}(\mathbf{x}_a, E) &= -\frac{N_0}{2\pi d_i} \sum_{m,n=0}^{\infty} \tilde{u}_{mn}^2(\mathbf{x}_a) \Theta_{mn} \\ &\quad \times \int_{-\infty}^{\infty} \frac{\tilde{R}_{ij} [\omega^2 + (B_{mn}^j)^2] + \frac{d_i}{d_j} \tilde{R}_{ji} \Gamma_{t,ij}^2}{[\omega^2 + (\varepsilon_{mn}^+)^2][\omega^2 + (\varepsilon_{mn}^-)^2]} d\omega. \end{aligned} \quad (\text{B1})$$

For the second iteration we keep first and second order terms in the expressions for $|A_{mn}^{i,j}|^2$:

$$\begin{aligned} S_{i,2}(\mathbf{x}_a, E) &= -2\text{Re} \sum_{m,n=0}^{\infty} \tilde{u}_{mn}(\mathbf{x}_a) \Theta_{mn} \\ &\quad \times \int_{-\infty}^{\infty} \frac{d\omega}{[\omega^2 + (\varepsilon_{mn}^+)^2][\omega^2 + (\varepsilon_{mn}^-)^2]} \\ &\quad \times \left\{ \tilde{\Phi}_{mn}^i(\mathbf{x}_a, \omega) \left[\tilde{R}_{ij} [\omega^2 + (B_{mn}^j)^2] + \frac{d_i}{d_j} \tilde{R}_{ji} \Gamma_{t,ij}^2 \right] \right. \\ &\quad + \tilde{\Phi}_{mn}^j(\mathbf{x}_a, \omega) \left[\frac{d_j}{d_i} \tilde{R}_{ij} \Gamma_{t,ij} [i\omega + (B_{mn}^j)] \right. \\ &\quad \left. \left. + \tilde{R}_{ji} \Gamma_{t,ij} (-i\omega + B_{mn}^i) \right] \right\}. \end{aligned} \quad (\text{B2})$$

Functions $\tilde{\Phi}_{mn}^{i,j}$ are analytic in the upper half of the complex ω plane. Thus, the integration in $S_{i,1}(\mathbf{x}_a, E)$ is straightforward and yields

$$\begin{aligned} S_{i,1}(\mathbf{x}_a, E) &= -\frac{N_0}{2d_i} \tilde{R}_{ij} \sum_{m,n=0}^{\infty} \tilde{u}_{mn}^2(\mathbf{x}_a) \Theta_{mn} \\ &\quad \times \frac{\left[(B_{mn}^j)^2 + \varepsilon_{mn}^+ \varepsilon_{mn}^- + \frac{d_i}{d_j} \tilde{R}_{ji} \Gamma_{t,ij}^2 \right]}{\varepsilon_{mn}^+ \varepsilon_{mn}^- (\varepsilon_{mn}^+ + \varepsilon_{mn}^-)}. \end{aligned} \quad (\text{B3})$$

After some tedious algebra we obtain the second iteration

$$\begin{aligned}
S_{i,2}(\mathbf{x}_a, E) = & -2\pi \sum_{m,n=0}^{\infty} \tilde{u}_{mn}(\mathbf{x}_a) \Theta_{mn} [(\varepsilon_{mn}^+)^2 - (\varepsilon_{mn}^-)^2]^{-1} \left\{ \frac{\tilde{\Phi}_{mn}^i(\mathbf{x}_a, i\varepsilon_{mn}^-)}{\varepsilon_{mn}^-} \left[\tilde{R}_{ij} [(B_{mn}^j)^2 - (\varepsilon_{mn}^-)^2] + \frac{d_i}{d_j} \tilde{R}_{ji} \Gamma_{t,ij}^2 \right] \right. \\
& - \frac{\tilde{\Phi}_{mn}^i(\mathbf{x}_a, i\varepsilon_{mn}^+)}{\varepsilon_{mn}^+} \left[\tilde{R}_{ij} [(B_{mn}^j)^2 - (\varepsilon_{mn}^+)^2] + \frac{d_i}{d_j} \tilde{R}_{ji} \Gamma_{t,ij}^2 \right] + \frac{\tilde{\Phi}_{mn}^j(\mathbf{x}_a, i\varepsilon_{mn}^-)}{\varepsilon_{mn}^-} \\
& \times \left[\tilde{R}_{ij} \frac{d_j}{d_i} \Gamma_{t,ji} (B_{mn}^j - \varepsilon_{mn}^-) + \tilde{R}_{ji} \Gamma_{t,ij} (B_{mn}^i + \varepsilon_{mn}^-) \right] - \frac{\tilde{\Phi}_{mn}^j(\mathbf{x}_a, i\varepsilon_{mn}^+)}{\varepsilon_{mn}^+} \\
& \left. \times \left[\tilde{R}_{ij} \frac{d_j}{d_i} \Gamma_{t,ji} (B_{mn}^j - \varepsilon_{mn}^+) + \tilde{R}_{ji} \Gamma_{t,ij} (B_{mn}^i + \varepsilon_{mn}^+) \right] \right\}, \tag{B4}
\end{aligned}$$

where, in accordance with Eqs. (14) and (15),

$$\begin{aligned}
\tilde{\Phi}_{mn}^i(\mathbf{x}_a, \omega) &= -\frac{R_i^* N_0^2 \Theta_{mn}^{-1}}{4\pi L d_i^2} \sum_{k,l=0}^{\infty} \tilde{u}_{kl}(\mathbf{x}_a) \tilde{u}_{m-k,n-l}(\mathbf{x}_a) \Theta_{kl} \\
& \times \frac{[C_{kl,mn}^{++}(\omega) + C_{kl,mn}^{--}(\omega) - C_{kl,mn}^{+-}(\omega) - C_{kl,mn}^{-+}(\omega)]}{(\varepsilon_{kl}^+ - \varepsilon_{kl}^-)(\varepsilon_{m-k,n-l}^+ - \varepsilon_{m-k,n-l}^-)}
\end{aligned}$$

and

$$C_{kl,mn}^{\pm\mp}(\omega) = \frac{(B_{kl}^j - \varepsilon_{kl}^{\pm})(B_{m-k,n-l}^j - \varepsilon_{m-k,n-l}^{\mp}) - \frac{d_i R_{ji}^*}{d_j R_i^*} \Gamma_{t,ij}^2}{-i\omega + \varepsilon_{kl}^{\pm} + \varepsilon_{m-k,n-l}^{\mp}}.$$

Similarly

$$\begin{aligned}
\tilde{\Phi}_{mn}^j(\mathbf{x}_a, \omega) &= -\frac{R_{ij}^* N_0^2 \Theta_{mn}^{-1}}{4\pi L d_i d_j} \sum_{k,l=0}^{\infty} \tilde{u}_{kl}(\mathbf{x}_a) \tilde{u}_{m-k,n-l}(\mathbf{x}_a) \Theta_{kl} \\
& \times \frac{[D_{kl,mn}^{++}(\omega) + D_{kl,mn}^{--}(\omega) - D_{kl,mn}^{+-}(\omega) - D_{kl,mn}^{-+}(\omega)]}{(\varepsilon_{kl}^+ - \varepsilon_{kl}^-)(\varepsilon_{m-k,n-l}^+ - \varepsilon_{m-k,n-l}^-)}
\end{aligned}$$

and

$$D_{kl,mn}^{\pm\mp}(\omega) = \frac{(B_{kl}^j - \varepsilon_{kl}^{\pm})(B_{m-k,n-l}^j - \varepsilon_{m-k,n-l}^{\mp}) - \frac{d_i R_{ji}^*}{d_j R_{ij}^*} \Gamma_{t,ij}^2}{-i\omega + \varepsilon_{kl}^{\pm} + \varepsilon_{m-k,n-l}^{\mp}}.$$

An estimate of the order of magnitude of $S_{i,1}$ can be obtained from the leading term ($n, m = 0$):

$$S_{i,1} \approx -\frac{2R_i^* n_0}{\Gamma_{t,ij} + \Gamma_{t,ji} + \Gamma_{l,i} + \Gamma_{l,j}}. \tag{B5}$$

The criterion for applicability of the iteration scheme $|S_{i,1}| \ll 1$ and $|S_{i,2}| \ll |S_{i,1}|$ then implies $R_i^* n_0 \ll \Gamma_{t,ij} + \Gamma_{t,ji} + \Gamma_{l,i} + \Gamma_{l,j}$, i.e., the quasiparticle recombination rate in the homo-

geneous state with quasiparticle density n_0 should be much slower than the total quasiparticle tunnel and loss rates.

APPENDIX C: DIFFUSION INTO LEADS AND BRIDGES

To discuss the effects of leads and bridges quantitatively, we consider the inhomogeneous diffusion equation in the dissipative medium

$$\frac{\partial n}{\partial t} - D \Delta n + \Gamma n = 4\pi \rho(\mathbf{x}, t). \tag{C1}$$

This equation is a simplified form of Eq. (7). The general solution of this equation is, see Ref. 25:

$$\begin{aligned}
n(\mathbf{x}, t) = & \int_0^t dt' \int d\mathbf{x}' \rho(\mathbf{x}', t') G(\mathbf{x}, t; \mathbf{x}', t') \\
& + \frac{1}{4\pi} \int_0^t dt' \int d\mathbf{x}' [G \nabla_{\mathbf{x}'} \cdot n - n \nabla_{\mathbf{x}'} \cdot G] \\
& + \frac{1}{4\pi D} \int d\mathbf{x}' [nG]_{t=0}. \tag{C2}
\end{aligned}$$

Here $n(\mathbf{x}, t)$ is the density of excess quasiparticles in the electrode, $4\pi \rho(\mathbf{x}, t) = N_0/d_i \delta(\mathbf{x} - \mathbf{x}_a) \delta(t)$ is the source density term and $G(\mathbf{x}, t; \mathbf{x}', t')$ is the Green function for the diffusion equation. Considering the quasiparticle diffusion following the photon absorption, we will drop the last term in Eq. (C2) describing the effect of initial conditions. The Green function $G(\mathbf{x}, t; \mathbf{x}', t')$ has to be calculated for a particular geometry with appropriate boundary conditions. The simplest case is two-dimensional diffusion in the bulk, where

$$G(\mathbf{x}, t; \mathbf{x}', t') = \frac{\Theta(t-t')}{Dt} \exp \left[-\frac{(\mathbf{x} - \mathbf{x}')^2}{4D(t-t')} - \frac{t-t'}{\tau} \right]. \tag{C3}$$

This Green function can be used to model the expansion of the quasiparticle distribution out of the absorption site during the initial period of time when the influence of edges is small. For a lead in the form of a semi-infinite bar with width

w_l and the lead mouth at $\mathbf{x}_l=0$ the Green function describing one-dimensional diffusion becomes

$$G(x,t;x',t') = \frac{2\pi D}{[\pi D(t-t')]^{\frac{1}{2}}} \left\{ \exp\left[-\frac{(x-x')^2}{4D(t-t')}\right] - \exp\left[-\frac{(x+x')^2}{4D(t-t')}\right] \right\} \exp\left(-\frac{t-t'}{\tau}\right). \quad (\text{C4})$$

Since the photon absorption takes place outside the lead, $\rho=0$, and because the lead is initially empty, only the second term in Eq. (C2) survives, so that

$$n(x,t) = \frac{x}{\sqrt{4\pi D}} \int_{-\infty}^t dt' \frac{n_0(t')}{(t-t')^{3/2}} \times \exp\left[-\frac{x^2}{4D(t-t')} - \gamma_l(t-t')\right], \quad (\text{C5})$$

where γ_l is the loss rate in the lead. Using Eq. (C5) to calculate the quasiparticle flux into the lead at the lead mouth, and applying the continuity equation for the quasiparticles in the electrode, we finally arrive at

$$\begin{aligned} \frac{\partial n}{\partial t} \Big|_{\text{diff,lead}} &= -\frac{w_l D_l}{L^2} \frac{\partial n}{\partial t} \Big|_{x=0} \\ &= \frac{L^2}{\sqrt{\tau_l}} \delta(x-x_l) \lim_{\epsilon \rightarrow 0} \left\{ \frac{1}{\epsilon} \int_0^\infty d\xi (1-2\xi^2) \right. \\ &\quad \left. \times \exp\left(-\xi^2 - \gamma_l \frac{\epsilon^2}{\xi^2}\right) \left\langle n\left(x, t - \frac{\epsilon^2}{\xi^2}\right) \right\rangle \right\}. \end{aligned} \quad (\text{C6})$$

Here $\tau_l = \pi L^4/w_l^2 D_l$ is a characteristic diffusion time for the lead, D_l is the quasiparticle diffusion coefficient inside the lead and $\langle n \rangle$ denotes the quasiparticle density averaged over the lead cross section. For the lead mouth located at the center of the STJ side $\langle n \rangle = 1/w \int_{-w/2}^{w/2} n dy$, whereas for a corner location $\langle n \rangle = 2/w^2 \int_{L/2-w/\sqrt{2}}^{L/2+w/\sqrt{2}} \int_{L/2-w/\sqrt{2}}^{L/2+w/\sqrt{2}} n dx dy$. Expanding the loss rate due to diffusion into the lead in harmonics of the square STJ, we obtain

$$\begin{aligned} \frac{\partial n}{\partial t} \Big|_{\text{diff,lead}} &= -L^2 \delta(x-x_l) \sum_{m,n=0}^{\infty} \langle u_{mn}(x) \rangle \\ &\quad \times \int_{-\infty}^{\infty} d\omega f_{mn}(\omega) \exp(-i\omega t) g_l(\omega), \end{aligned} \quad (\text{C7})$$

where we have introduced the function $g_l(\omega) = \sqrt{\pi(\gamma_l - i\omega)} \tau_l^{-1}$ to describe the effect of quasiparticle diffusion into the lead. To arrive at this formula we have used the following result:

$$\begin{aligned} \lim_{\epsilon \rightarrow 0} \left\{ \frac{1}{\epsilon} \int_0^\infty d\xi (1-2\xi^2) \exp\left[-\xi^2 + \left(i\omega - \gamma_l \frac{\epsilon^2}{\xi^2}\right)\right] \right\} \\ = -\sqrt{\pi(\gamma_l - i\omega)}. \end{aligned} \quad (\text{C8})$$

For a narrow rectangular bridge of length d_b and width w_b at the coordinate \mathbf{x}_b it is most convenient to expand the Green function in terms of corresponding eigenfunctions. Performing exactly the same calculations as earlier for semi-infinite lead and introducing the characteristic diffusion time for the bridge connection $\tau_b = \pi L^4/w_b^2 D_b$, where D_b is diffusion coefficient in the bridge, we obtain instead of Eq. (C6)

$$\begin{aligned} \frac{\partial n}{\partial t} \Big|_{\text{diff,bridge}} &= -\frac{w_b D_b}{L^2} \frac{\partial n}{\partial t} \Big|_{x=d/2} \\ &= \frac{L^2}{\sqrt{\tau_b}} \delta(x-x_b) \frac{4\sqrt{D_b}}{d_b} \int_{d_b/4\sqrt{D_b}}^\infty d\xi (1-2\xi^2) \\ &\quad \times \exp\left(-\xi^2 - \gamma_b \frac{d_b^2}{16D_b \xi^2}\right) \\ &\quad \times \left[\left\langle n^-\left(x, t - \frac{d_b^2}{16D_b \xi^2}\right) \right\rangle \right. \\ &\quad \left. - \left\langle n^+\left(x, t - \frac{d_b^2}{16D_b \xi^2}\right) \right\rangle \right], \end{aligned} \quad (\text{C9})$$

where $\langle n^\mp \rangle$ are quasiparticle densities on the left and on the right of the bridge respectively, and γ_b is the quasiparticle loss rate in the bridge. In most practically important cases the bridge may be considered as short, in the sense that the diffusion time across the bridge is small compared to the time scales governing the evolution of the quasiparticle distribution in the STJ. In this case, upon taking the limit $d_b \rightarrow 0$ and keeping only the principal terms in Eq. (C9), one obtains a similar result to Eq. (C7) with the only difference being the counter flux from the right of the bridge

$$\begin{aligned} \frac{\partial n}{\partial t} \Big|_{\text{diff,bridge}} &= -L^2 \delta(\mathbf{x}-\mathbf{x}_b) \sum_{m,n=0}^{\infty} \langle u_{mn}(\mathbf{x}) \rangle \\ &\quad \times \int_{-\infty}^{\infty} d\omega [f_{mn}^-(\omega) - f_{mn}^+(\omega)] \\ &\quad \times \exp(-i\omega t) g_b(\omega), \end{aligned} \quad (\text{C10})$$

where $g_b(\omega) = \sqrt{\pi(\gamma_b - i\omega)} \tau_b^{-1}$ and, as earlier, the superscripts \mp refer to the harmonics on the left and right of the bridge, respectively. It immediately follows from Eqs. (C7) and (C10) that one cannot describe the effects of leads and bridges by simply introducing another quasiparticle loss rate. The quasiparticle loss in the electrode due to diffusion into leads and across the bridges is a nonexponential process. With the Eqs. (C7) and (C10) we can now derive $S_{i,\text{leads}}(E, \mathbf{x}_a)$ and $S_{i,\text{bridge}}(E, \mathbf{x}_a)$. First, it follows from Eq. (16) that to find the charge response and then the normalized

response we need to know only the Fourier components of harmonics $f_{mn}(\mathbf{x}_a, \omega)$ taken at $\omega=0$. Thus we take the Fourier transform of the main system of equations (11), ignore the nonlinear terms, keep the loss terms into leads and bridges, Eqs. (C7) and (C10), and take $\omega=0$. We stress that the effect of bridges and leads on the charge output and STJ response is fully accounted for by a single parameter per bridge(lead), namely, $g_{b(l)}(\omega=0) \equiv g_{b(l)} = \sqrt{\pi \gamma_{b(l)} \tau_{b(l)}^{-1}}$. Assuming that the bridge connections exist only to the base electrode, we then obtain

$$\begin{aligned}
& B_{mn}^i f_{mn}^i(0) - \Gamma_{t,ji} \frac{d_j}{d_i} f_{mn}^j(0) \\
& + \Theta_{mn} L^2 g_{l,i} u_{mn}(\mathbf{x}_{l,i}) \sum_{k,l=0}^{\infty} \langle u_{kl}(\mathbf{x}_{l,i}) \rangle f_{kl}^i(0) \\
& + \Theta_{mn} L^2 \sum_{\nu} g_{b,\nu} u_{mn}(\mathbf{x}_{b,\nu}) \sum_{k,l=0}^{\infty} \langle u_{kl}(\mathbf{x}_{b,\nu}) \rangle f_{kl}^i(0) \\
& = \frac{N_0}{2\pi d_i} u_{mn}(\mathbf{x}_a), \\
& B_{mn}^j f_{mn}^j(0) - \Gamma_{t,ij} \frac{d_i}{d_j} f_{mn}^i(0) \\
& + \Theta_{mn} L^2 g_{l,j} u_{mn}(\mathbf{x}_{l,j}) \sum_{k,l=0}^{\infty} \langle u_{kl}(\mathbf{x}_{l,j}) \rangle f_{kl}^j(0) \\
& = \frac{N_0}{2\pi d_j} u_{mn}(\mathbf{x}_a), \tag{C11}
\end{aligned}$$

where $f_{mn}^{i(j)}(0) \equiv f_{mn}^{i(j)}(\mathbf{x}_a, \omega=0)$ and ν labels the bridges on the base electrode. We introduce

$$\begin{aligned}
p_{l,i} &= \sum_{k,l=0}^{\infty} \langle u_{kl}(\mathbf{x}_{l,i}) \rangle f_{kl}^i(0), \\
p_{l,j} &= \sum_{k,l=0}^{\infty} \langle u_{kl}(\mathbf{x}_{l,j}) \rangle f_{kl}^j(0), \\
p_{b,\nu} &= \sum_{k,l=0}^{\infty} \langle u_{kl}(\mathbf{x}_{b,\nu}) \rangle f_{kl}^i(0). \tag{C12}
\end{aligned}$$

It is clear that using the system (C11) we can easily obtain a finite linear algebraic system for the variables $p_{l,i}, p_{l,j}, p_{b,\nu}$. The solution of this system is straightforward. Subsequent substitution of the results into Eq. (C11) yields all harmonics $f_{mn}^{i(j)}(0)$. Finally, the result for the response acquires the form

$$\begin{aligned}
S_{\text{leads+bridges}}^{\text{base}}(\mathbf{x}_a) &= -\frac{2L^2 \pi d_i}{N_0} \left[g_{l,i} p_{l,i} + \sum_{\nu} g_{b,\nu} p_{b,\nu} \right] \\
& - \frac{2L^2 \pi d_j}{N_0} \frac{\Gamma_{t,ji}}{\Gamma_{t,ij}} \frac{2\Gamma_{t,ij} + \Gamma_{l,i}}{2\Gamma_{t,ji} + \Gamma_{l,j}} g_{l,j} p_{l,j} \\
& \tag{C13}
\end{aligned}$$

and

$$\begin{aligned}
S_{\text{leads+bridges}}^{\text{top}}(\mathbf{x}_a) &= -\frac{2L^2 \pi d_i}{N_0} g_{l,i} p_{l,i} \\
& - \frac{2L^2 \pi d_j}{N_0} \frac{\Gamma_{t,ji}}{\Gamma_{t,ij}} \frac{2\Gamma_{t,ij} + \Gamma_{l,i}}{2\Gamma_{t,ji} + \Gamma_{l,j}} \\
& \times \left[g_{l,i} p_{l,i} + \sum_{\nu} g_{b,\nu} p_{b,\nu} \right]. \tag{C14}
\end{aligned}$$

Using the solutions of Eq. (C11) we can easily find the quasiparticle density in any of the neighboring electrodes due to cross talk over the bridge connections. This yields

$$S_{\text{cross talk}, \nu}(\mathbf{x}_a) = \frac{2L^2 \pi d_i}{N_0} g_{b,\nu} p_{b,\nu}. \tag{C15}$$

Finally, we point out that although we have not specifically dealt with local traps, it may be clear from the above analysis that traps, leads and bridges all belong to the same family of localized loss channels, characterized by one parameter g_{ν} .

APPENDIX D: IMPERFECTLY REFLECTING EDGES

Following Refs. 14,16 the model assumption is that the quasiparticle losses at the edges of an electrode can be described by a single edge-quality parameter β_i . In Ref. 14 β_i is related to $R_{i,\text{edge}}$, the edge reflectivity, or the probability that a quasiparticle is trapped upon hitting the edge, as

$$\beta_i = \frac{3L}{4\lambda_i} (1 - R_{i,\text{edge}}), \tag{D1}$$

where λ_i is the electron mean free path in electrode i . In general $\beta_i \neq \beta_j$, even when the edge reflectivity $R_{i,\text{edge}}$ is the same in both electrodes, because $\beta_{i(j)}$ also depend on the accessibility of the edges, i.e., the diffusive properties of the quasiparticles. An example is the case of STJ's with an epitaxial base electrode and a polycrystalline top electrode. Because $R_{i,\text{edge}}$ depends on details of the processing route, it may be considered identical for both electrodes; however, the diffusion coefficients may differ by an order of magnitude.

Let $\{u_{mn}^j(\mathbf{x})\}$ be the complete set of orthogonal eigenfunctions, which are solutions of the Helmholtz equations for each electrode with the following boundary conditions:

$$[\beta_j u_{mn}^j + \hat{\mathbf{e}} \nabla u_{mn}^j]_{\text{edge}} = 0, \tag{D2}$$

where $\hat{\mathbf{e}}$ is the unit vector normal to the corresponding edge of the STJ. The solution of Helmholtz problem with the boundary conditions (D2) is

$$\begin{aligned}
u_{mn}^j(x,y) &= \frac{2}{L} \left[\left(1 + \frac{2\beta_j}{\beta_j^2 + k_{j,m}^2 L^2} \right) \left(1 + \frac{2\beta_j}{\beta_j^2 + k_{j,n}^2 L^2} \right) \right]^{-1/2} \\
& \times \sin\left(\frac{m\pi}{2} + k_{j,m} x\right) \sin\left(\frac{n\pi}{2} + k_{j,n} y\right), \tag{D3}
\end{aligned}$$

where $k_{j,m}$ is the solution of the dispersion equation

$$k_{j,m}L = m\pi - 2 \arctan\left(\frac{k_{j,m}L}{\beta_j}\right). \quad (\text{D4})$$

Note that to compare Eq. (D3) with Eq. (A5) for the ideal edge limit $\beta \rightarrow 0$ we have to make a shift in Eq. (D3): $n \rightarrow n+1, m \rightarrow m+1$, so that the eigenfunctions in Eq. (D3) belong to similar eigenvalues. Then $\sin(m\pi/2 + k_{j,m}x) \rightarrow \cos(m\pi/2 + k_{j,m+1}x)$ and Eq. (D3) coincides with Eq. (A5) in the ideal edge limit. Evenly spaced harmonics $u_{mn}^i(\mathbf{x})$ from one electrode and $u_{mn}^j(\mathbf{x})$ from the other are not orthogonal. As a result, the system of Rothwarf-Taylor equations, when expanded into harmonics, becomes an infinite system of coupled equations with cross-coupling terms due to the nonorthogonal harmonics. Their contributions, however, become negligible for high-quality STJ's, in which the edge losses are small. Quantitatively, this is the case when $\pi^{-2}|\beta_i - \beta_j| \ll 1$. Neglecting all cross-coupling terms to this accuracy we obtain exactly the same equations for the harmonics as the linearized system (11). After some simple algebra, which differs slightly from the derivation in Appendix A due to the expansion into two different sets of eigenfunctions, we obtain

$$S_{i,\text{edge}}(E, \mathbf{x}_a) = \frac{8\Gamma_{t,ij}L}{\langle n_i \rangle} \sum_{m,n=0}^{\infty} \frac{\tilde{u}_{mn}(\mathbf{x}_a)}{\tilde{\epsilon}_{mn}^+ \tilde{\epsilon}_{mn}^-} [\beta_i^2 \tilde{B}_{mn}^j F_m^i F_n^i + \beta_j^2 \Gamma_{t,ji} F_m^j F_n^j] - 1, \quad (\text{D5})$$

where

$$F_m^i = \frac{1}{u_m^i [\beta_i^2 + 2\beta_i + (u_m^i)^2]^{1/2}}.$$

In Eq. (D5) we used the notation $u_m^i \equiv k_{2m+1}^i$ to make the comparison with the results of Refs. 14 and 16 straightforward and also $\tilde{u}_{mn}(\mathbf{x}) \equiv u_{2m+1,2n+1}^i$, $\tilde{\epsilon}_{mn}^{\pm} \equiv \epsilon_{2m+1,2n+1}^{\pm}$, $\tilde{B}_{mn} \equiv B_{2m+1,2n+1}$. The results of the model considered in Ref. 14 immediately follow from Eq. (D5) by taking $\Gamma_{t,ji} = 0$, while the results of Ref. 16 are obtained by taking $\beta_i = \beta_j$.

APPENDIX E: TIME-DEPENDENT SOLUTION OF THE BALANCE EQUATIONS

The general solution of the balance equations (11) permits an iteration scheme which is obtained by assuming nonlinear terms as known entries:

$$\begin{aligned} f_{mn}^i &= \frac{2\pi\Theta(t)\Theta_{mn}}{\epsilon_{mn}^+ - \epsilon_{mn}^-} \left\{ \frac{N_{0\sim}}{d_i} u_{mn}(\mathbf{x}_a) [(B_{mn}^j - \epsilon_{mn}^-) e^{-\epsilon_{mn}^- t} - (B_{mn}^j - \epsilon_{mn}^+) e^{-\epsilon_{mn}^+ t}] + (B_{mn}^j - \epsilon_{mn}^-) e^{-\epsilon_{mn}^- t} \right. \\ &\quad \times \int_0^t e^{\epsilon_{mn}^- t'} \Phi_{mn}^i(\mathbf{x}_a, t') dt' - (B_{mn}^j - \epsilon_{mn}^+) e^{-\epsilon_{mn}^+ t} \int_0^t e^{\epsilon_{mn}^+ t'} \Phi_{mn}^i(\mathbf{x}_a, t') dt' \\ &\quad \left. - \frac{d_j}{d_i} \Gamma_{t,ji} \left[e^{-\epsilon_{mn}^- t} \int_0^t e^{\epsilon_{mn}^- t'} \Phi_{mn}^j(\mathbf{x}_a, t') dt' - e^{-\epsilon_{mn}^+ t} \int_0^t e^{\epsilon_{mn}^+ t'} \Phi_{mn}^j(\mathbf{x}_a, t') dt' \right] \right\}, \\ f_{mn}^j &= \frac{d_j}{d_j} \Theta(t)\Theta_{mn} \frac{2\pi\Gamma_{t,ij}}{\epsilon_{mn}^+ - \epsilon_{mn}^-} \left\{ \frac{N_{0\sim}}{d_i} u_{mn}(\mathbf{x}_a) [e^{-\epsilon_{mn}^- t} - e^{-\epsilon_{mn}^+ t}] + e^{-\epsilon_{mn}^- t} \int_0^t e^{\epsilon_{mn}^- t'} \Phi_{mn}^i(\mathbf{x}_a, t') dt' \right. \\ &\quad - e^{-\epsilon_{mn}^+ t} \int_0^t e^{\epsilon_{mn}^+ t'} \Phi_{mn}^i(\mathbf{x}_a, t') dt' - \frac{d_j}{d_i \Gamma_{t,ij}} \left[(B_{mn}^i - \epsilon_{mn}^+) e^{-\epsilon_{mn}^+ t} \int_0^t e^{\epsilon_{mn}^+ t'} \Phi_{mn}^j(\mathbf{x}_a, t') dt' \right. \\ &\quad \left. \left. - (B_{mn}^i - \epsilon_{mn}^-) e^{-\epsilon_{mn}^- t} \int_0^t e^{\epsilon_{mn}^- t'} \Phi_{mn}^j(\mathbf{x}_a, t') dt' \right] \right\}. \quad (\text{E1}) \end{aligned}$$

The zeroth order iteration is given by Eq. (E1), which is obtained by ignoring all nonlinear terms with functions $\Phi_{mn}^{i,j}$. The next order iteration is straightforward to implement. These solutions can be used to find $Q_{i,1}(E, \mathbf{x}_a, t)$, $Q_{i,2}(E, \mathbf{x}_a, t)$ and higher order terms. The calculations are simple but the results are too cumbersome to present fully here. We give only the expression for the ideal solution, integrated over the area of the STJ:

$$Q_{0,i}(E, t) = eN_0 \left[\langle n_i \rangle + \frac{\Gamma_{t,ij}(B_{00}^j - \epsilon_{00}^+ + \Gamma_{t,ji})}{(\epsilon_{00}^+ - \epsilon_{00}^-) \epsilon_{00}^+} \exp(-\epsilon_{00}^+ t) - \frac{\Gamma_{t,ij}(B_{00}^j - \epsilon_{00}^- + \Gamma_{t,ji})}{(\epsilon_{00}^+ - \epsilon_{00}^-) \epsilon_{00}^-} \exp(-\epsilon_{00}^- t) \right]. \quad (\text{E2})$$

When differentiated with respect to time, it provides a (usually) good approximation to the shapes of the current pulse produced by the STJ as a function of time.

- ¹J.C. Mather, *Nature (London)* **401**, 654 (1999).
- ²U. Fano, *Phys. Rev.* **72**, 26 (1947).
- ³D.J. Goldie, P.L. Brink, C. Patel, N.E. Booth, and G.L. Salmon, *Appl. Phys. Lett.* **64**, 3169 (1994).
- ⁴C. Mears, S.E. Labov, and A. Barfknecht, *Appl. Phys. Lett.* **63**, 2961 (1993).
- ⁵S. Friedrich, J.B. le Grand, L.J. Hiller, J. Kipp, M. Frank, S.E. Labov, S.P. Cramer, and A.T. Barfknecht, *IEEE Trans. Appl. Supercond.* **9**, 3330 (1998).
- ⁶J. Martin *et al.*, *Nucl. Instrum. Methods Phys. Res. A* **370**, 88 (1996).
- ⁷H. Pressler, M. Ohkubo, M. Koike, T. Zama, T. Nakamura, and M. Katagiri, *Appl. Phys. Lett.* **77**, 4055 (2000).
- ⁸P. Verhoeve, N. Rando, A. Peacock, A. van Dordrecht, A. Poelaert, D.J. Goldie, and R. Venn, *J. Appl. Phys.* **83**, 6118 (1998).
- ⁹P. Verhoeve *et al.*, *Phys. Rev. B* **53**, 809 (1996).
- ¹⁰A. Peacock, P. Verhoeve, N. Rando, M.A.C. Perryman, B.G. Taylor, and P. Jakobsen, *Astron. Astrophys.* **123**, 581 (1997).
- ¹¹S. Kraft, A. Peacock, M. Bavdaz, B. Castelletto, B. Collaudin, and D. Perez, *Proc. SPIE* **3445**, 226 (1998).
- ¹²A. Rothwarf and B.N. Taylor, *Phys. Rev. Lett.* **19**, 27 (1967).
- ¹³J.B. le Grand, Ph.D. thesis, Utrecht University, 1994.
- ¹⁴O.J. Luiten, M.L. van den Berg, J. Gomez Rivas, M.P. Bruijn, F.B. Kiewiet, and P.A.J. de Korte (unpublished).
- ¹⁵R. Christiano *et al.*, *J. Appl. Phys.* **86**, 4580 (1999).
- ¹⁶L. Parlato *et al.*, *Nucl. Instrum. Methods Phys. Res. A* **440**, 15 (2000).
- ¹⁷R. den Hartog, A.G. Kozorezov, J.K. Wigmore, D. Martin, P. Verhoeve, A. Peacock, A. Poelaert, and G. Brammertz, following paper, *Phys. Rev. B* **66**, 094511 (2002).
- ¹⁸P. de Korte *et al.*, *Proc. SPIE* **1743**, 24 (1992).
- ¹⁹S. Kaplan *et al.*, *Phys. Rev. B* **14**, 4854 (1976).
- ²⁰S. Kaplan, *J. Low Temp. Phys.* **37**, 343 (1979).
- ²¹A. Poelaert, A. Peacock, N. Rando, P. Verhoeve, and P. Videler, *J. Appl. Phys.* **79**, 2574 (1996).
- ²²A. Kozorezov *et al.*, *Phys. Rev. B* **61**, 11 807 (2000).
- ²³R.H. den Hartog, P. Verhoeve, A. Peacock, A. Poelaert, and N. Rando, *IEEE Trans. Appl. Supercond.* **9**, 4495 (1999).
- ²⁴A. Poelaert, Ph.D. thesis, Twente University, 1999, Chap. 2.
- ²⁵P.M. Morse, H. Feshbach, *Methods of Theoretical Physics* (McGraw-Hill, New York 1953), Pt. I.
- ²⁶A. Poelaert, P. Verhoeve, N. Rando, A. Peacock, D.J. Goldie, and R. Venn, *Proc. SPIE* **2808**, 523 (1996).
- ²⁷R.H. den Hartog *et al.*, *Proc. SPIE* **4012**, 237 (2000).